Journal of Structural Geology 32 (2010) 507–522

Contents lists available at ScienceDirect

Journal of Structural Geology

journal homepage: www.elsevier.com/locate/jsg

Impact of ephemeral cataclastic fabrics on laser diffraction particle size distribution analysis in loose carbonate fault breccia

Fabrizio Storti*, Fabrizio Balsamo

Dipartimento di Scienze Geologiche, Università "Roma Tre", Largo S.L. Murialdo 1, I-00146 Roma, Italy

ARTICLE INFO

Article history:
Received 12 December 2008
Received in revised form
19 January 2010
Accepted 25 February 2010
Available online 4 March 2010

Keywords:
Fault breccia
Particle size
Particle shape
Laser diffraction granulometry
Particle disintegration
Cataclasis

ABSTRACT

Modern laser diffraction particle size analysers provide the possibility of fast particle size data acquisition over a wide size range by using a variety of analytical methods, named standard operating procedures. We performed specific tests on poorly coherent carbonate platform cataclastic rocks from a fault zone in the Central Apennines, Italy, by combining laser diffraction granulometry, thin section analysis, and optical morphometry. During laser diffraction granulometry tests, we used several wet and dry operating procedures that included different pump speeds, analyses with and without sample ultrasonication, and different dispersant liquids. The variability of particle size distributions from a given sample, as a function of the adopted operating procedure, has the same magnitude as that theoretically predicted in natural cataclastic rocks, from low- to high-deformation shear zones. Thin section image analysis and optical morphometry support mechanical disintegration of internally microfractured coarser particles in ephemeral cataclastic fabrics as the major cause of such a size variability.

1. Introduction

Cataclastic rocks exert a primary control on the frictional strength, stability, seismic velocity, and permeability properties of fault zones (Tullis and Weeks, 1986; Sammis et al., 1987; Marone and Scholz, 1989; Marone and Kilgore, 1993; Hadizadeh, 1994; Antonellini and Aydin, 1995; Caine et al., 1996; Evans et al., 1997; Ben-Zion and Sammis, 2003; Anthony and Marone, 2005; Reches and Dewers, 2005; Billi and Di Toro, 2008). Particle size distributions are central to these studies and have been widely used to investigate on the evolution of cataclasis (Borg et al., 1960; Engelder, 1974; Sammis et al., 1986, 1987; Blenkinsop, 1991; Morgan, 1999; Mair et al., 2002; Monzawa and Otsuki, 2003; Storti et al., 2003; Wilson et al., 2005; Heilbronner and Keulen, 2006; Fossen et al., 2007; Sammis and King, 2007; Sammis and Ben Zion, 2008; Torabi et al., 2008). Despite the large amount of available data, interpretation of particle size distributions from poorly cohesive cataclastic rocks is still controversial, particularly because results from microscopic and sieve analyses (e.g. Sammis et al., 1986; Billi and Storti, 2004), and from laser diffraction granulometry (e.g. Wilson et al., 2005; Reches and Dewers, 2005) have been used to support either fractal or non fractal behaviors, respectively. In power law particle size distributions, different fractal dimensions D correspond to different fragmentation mechanisms (Blenkinsop, 1991) and their spatial variability can be used to make inferences on the time variability of comminution mechanisms within fault cores (e.g. Storti et al., 2003). Given the fundamental importance of grain fragmentation on fault friction (e.g. Paterson and Wong, 2005) and hydrology (e.g. Zhang and Tullis, 1998), further studies are necessary to better understand the main reasons governing the difference between results obtained from microscopic and sieve analyses, and from laser diffraction granulometry, respectively.

A possible investigation strategy relies on the interplay between grain weakness in poorly cohesive fault rocks (e.g. Mair and Abe, 2008), and sample biasing associated with different particle size measurement techniques. Careful thin sectioning of epoxy-impregnated samples ensures negligible alteration and reliable grain size data in two dimensions (e.g. Panozzo, 1982). Both sieving and laser diffraction provide indirect measurements of spherically equivalent particle size distributions. Laser diffraction particle size analysers, however, ensure much more effective sampling strategies because they cover a wide size range, need short analysis time, and require very small amounts of material (e.g. Beuselinck et al., 1998), thus facilitating very detailed studies of particle size distributions in fault zones. Laser diffraction particle size analysers provide a wide variety of operating procedures that include the use of wet and dry dispersion units, of different dispersant agents, and/or ultrasonication to aid sample disgregation and dispersion,

* Corresponding author.
E-mail address: storti@uniroma3.it (F. Storti).

0191-8141/$ – see front matter © 2010 Elsevier Ltd. All rights reserved.
doi:10.1016/j.jsg.2010.02.006

the selection of the pump speed, the length of the measurement time, the number of measurement runs etc. (e.g. Blott et al., 2004; Sperazza et al., 2004). Such a variability of both technical and methodological factors, raises the question of their influence on measured results. Sample ultrasonication can aid particle disgregation by collision (e.g. Blott et al., 2004) and, consequently, it can produce a possible bias on particle size distributions, particularly on fault core rocks, where particles are mechanically weakened by fracturing. As a consequence, models of rock fragmentation based on data obtained from laser diffraction granulometry (e.g. Wilson et al., 2005; Reches and Dewers, 2005) might be influenced by the adopted operating procedures.

To further investigate on this, we adopted a twofold working strategy that includes the study of poorly cohesive carbonate cataclastic rocks in terms of their internal fabric, and of the response of such a fabric to different operating procedures in laser diffraction particle size analysers. We sampled cataclastic rocks in the core of the active Assergi extensional fault system (e.g. D'Agostino et al., 1998), which bounds to the south the Gran Sasso Massif in the Central Apennines, Italy (Fig. 1). The complex structural architecture in the cataclastic fault core of this fault system is characterized by incipient calcite cementation at the fault core-footwall damage zone transition, which allowed sampling for thin section analysis, and by loose breccias bounding intensely fractured shear lenses, which were sampled for laser diffraction and morphometric analyses. Thin section analysis was used to provide the 2D particle size distribution of the cataclastic fabric, aimed at investigating the role that abundant intragranular fracturing may play on data obtained by laser diffraction particle size analysers. Particle shape analysis was also used for morphometric grain characterization before and after laser diffraction analyses. Our results indicate a significant dependence of particle size data on the adopted analytical procedures in laser diffraction granulometry.

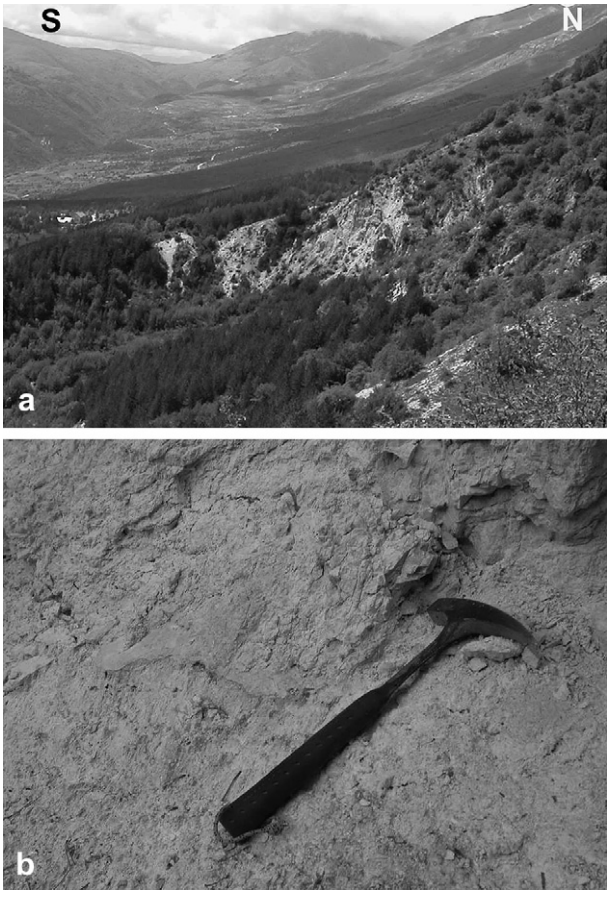

Fig. 1. (a) General view of the Assergi Basin, bounded to the north by the Assergi extensional fault system. The studied carbonate fault breccia was sampled in the fault core natural section exposed in the poorly vegetated ridge (42°21′03″N; 13°16′36″E). (b) Detail of the studied fault breccia. Loose material was sampled in the hammer area, while the poorly cemented one (which was then epoxy-impregnated for thin sectioning) was sampled in the area ahead of the hammer.

2. Thin section analysis

A representative thin section image of the cataclastic fabric in the Assergi extensional fault system is shown in Fig. 2a. A typical feature of the cataclastic fabric is intense microfracturing characterizing coarser clasts embedded in a finer matrix where strongly comminuted shear bands are abundant (Fig. 3). Gray scale digital microphotographs of four selected sub-areas were acquired for automated particle size distribution analysis by the Optimas 6.51™ image analysis software. Both actual and manually modified particle size distributions were computed. In the first case, manual retouching of the automatically detected fabric was used only to separate touching particles (Rawling and Goodwin, 2003; Storti et al., 2007). In the second case, retouching consisted of manually splitting larger clasts into constitutive fragments by exploiting all intragranular fractures clearly resolvable in the parent clasts. Plotting particle numbers versus size in bilogarithmic graphs allowed us to calculate the corresponding two dimensional fractal dimensions of both distributions as the slope of the best fit lines (e.g. Blenkinsop, 1991). Cumulative particle size distributions obtained by merging data from the four sub-images are shown in the bilogarithmic graph of Fig. 2b. Although producing an exhaustive scale-independent analysis was not our purpose in this work, data are well aligned along a best fit line in the 10 μm to 2000 μm size range, having a slope $D = 1.52$, which is quite similar to what obtained from wider observation ranges (e.g. Sammis et al., 1986). When transformed into a 3D value by adding 1 (Turcotte, 1986; Sammis et al., 1987), $D = 2.52$ fits very well in the range of fractal dimensions obtained from natural bulk cataclastic bodies (e.g. Sammis et al., 1986; Billi and Storti, 2004). Results after manual splitting coarser particles show a still satisfactory fit in a bilogarithmic graph, with a best fit line slope $D = 1.87$ (Fig. 2c). The corresponding three-dimensional value $D = 2.87$ falls in the typical range of localised cataclastic shear bands (e.g. Marone and Scholz, 1989; Storti et al., 2003; Billi and Storti, 2004).

Two gray scale digital microphotographs from the same thin section were also acquired at higher magnifications (Fig. 3a, b) to carefully draw the perimeter of 12 coarser clasts (equivalent diameter >1000 μm). For each clast we drew the perimeter of all the constitutive fracture-bounded fragments clearly resolvable in the images. Automated image analysis of the line drawings provided equivalent diameters of both parent clasts and pertaining fragments. Plotting these data permitted the analysis of the number of fragments as a function of the parent clast size and the size distribution of the fragment themselves (Fig. 3c). A great number of fragments in all parent clasts have equivalent diameters smaller than about 300 μm. Eight of the twelve analysed clasts have the majority of constitutive fragments showing equivalent diameters smaller than about 100 μm (Fig. 3d).

3. Laser diffraction granulometry

3.1. Instrument overview

Granulometric analyses were performed with a Mastersizer 2000 laser diffraction particle size analyser and associated

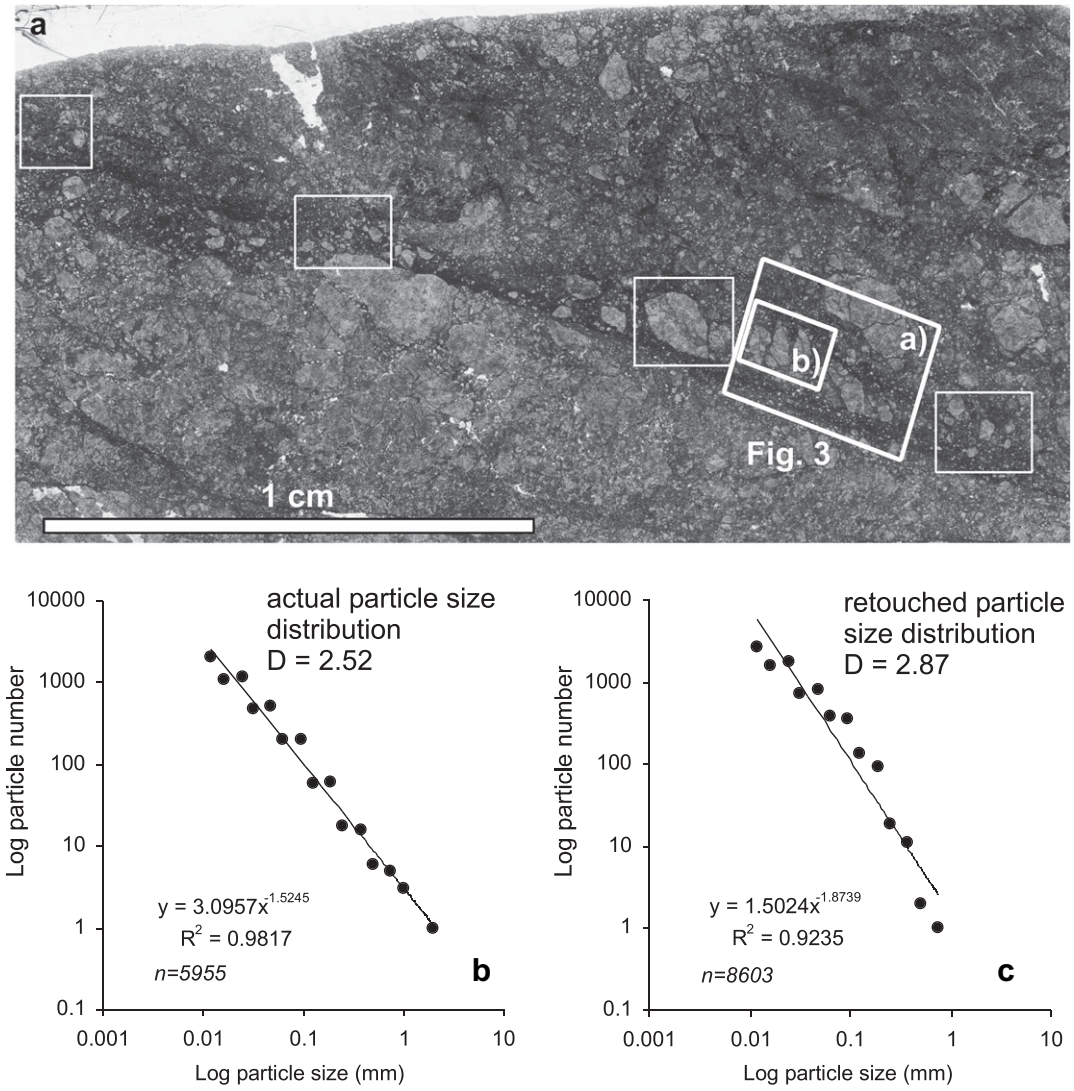

Fig. 2. (a) Digital image of the thin section used for studying 2D particle size distribution. The image was acquired by a Nikon Super Coolscan 5000 ED film scanner, at 4000 dpi resolution. The four sub-areas selected for the image analysis study are outlined by white boxes. Location of the sub-area used in Fig. 3 is also indicated. (b) Particle number versus size bilogarithmic graph of the actual particle size distribution obtained by merging data from the selected four sub-areas. The best fit line of the power law distribution provides a three-dimensional fractal dimension $D = 2.52$. (c) Particle number versus size bilogarithmic graph of the manually retouched particle size distribution obtained by merging data from the selected four sub-areas. The best fit line of the power law distribution provides a three-dimensional fractal dimension $D = 2.87$.

dispersion units, manufactured by Malvern Instruments Ltd. The instrument is designed for measuring particle sizes in the 0.02–2000 μm range by using a blue (488.0 μm wavelength LED) and red (633.8 μm wavelength He–Ne laser) light dual-wavelength, single-lens detection system. The light energy diffracted by the dilute suspension circulating through the cell is measured by 52 sensors. Light scattering data are accumulated in 100 size fractions bins, which are analysed at 1000 readings per second, and compiled with Malvern's Mastersizer 2000 software by using either full Mie or Fraunhofer diffraction theories (de Boer et al., 1987). Mie Theory, in particular, provides the most rigorous solution based on Maxwell's electromagnetic field equations and on the assumptions that: (1) particles are spherical; (2) suspension dilution guarantees that light scattered by one particle is measured before being-re-scattered by other particles; (3) the optical properties of particle and dispersion medium are known; (4) particles are homogeneous. Analyses performed for this work by the Mastersizer 2000 granulometer were all calculated using the Mie Theory. Sample preparation before analysis was performed by a Quantachrome sieving riffler-rotary sample splitter to automatically produce smaller representative sub-samples. We repeated sample splitting up to about 20 g weight, from which we took the analysed sub-sample aliquots (between 0.4 and 0.5 g for carbonate breccias and laser obscuration values between 10% and 15%, respectively).

We measured particle size distributions of carbonate particles mainly as wet dispersions using the Hydro 2000 MU sample dispersion unit, which has a capacity of 600–1000 ml using standard laboratory beakers. The dispersion mechanism consists of a “dip-in” sample recirculation head with built-in stirrer and sample recirculation centrifugal pump (from 600 to 4000 revolutions per minute, in the following rpm), and a continuously variable ultrasonic probe (maximum power is 20 μm of tip displacement). We also used the Scirocco 2000 dispersion unit to perform dry analyses. Particle flow in this unit is controlled using a variable feed-rate vibrating tray. Material dispersion is achieved by accelerating particles within a compressed air stream, together with particle and wall collision. The control of dispersive air pressure is to 2000 Pa over a range of 0–400,000 Pa.

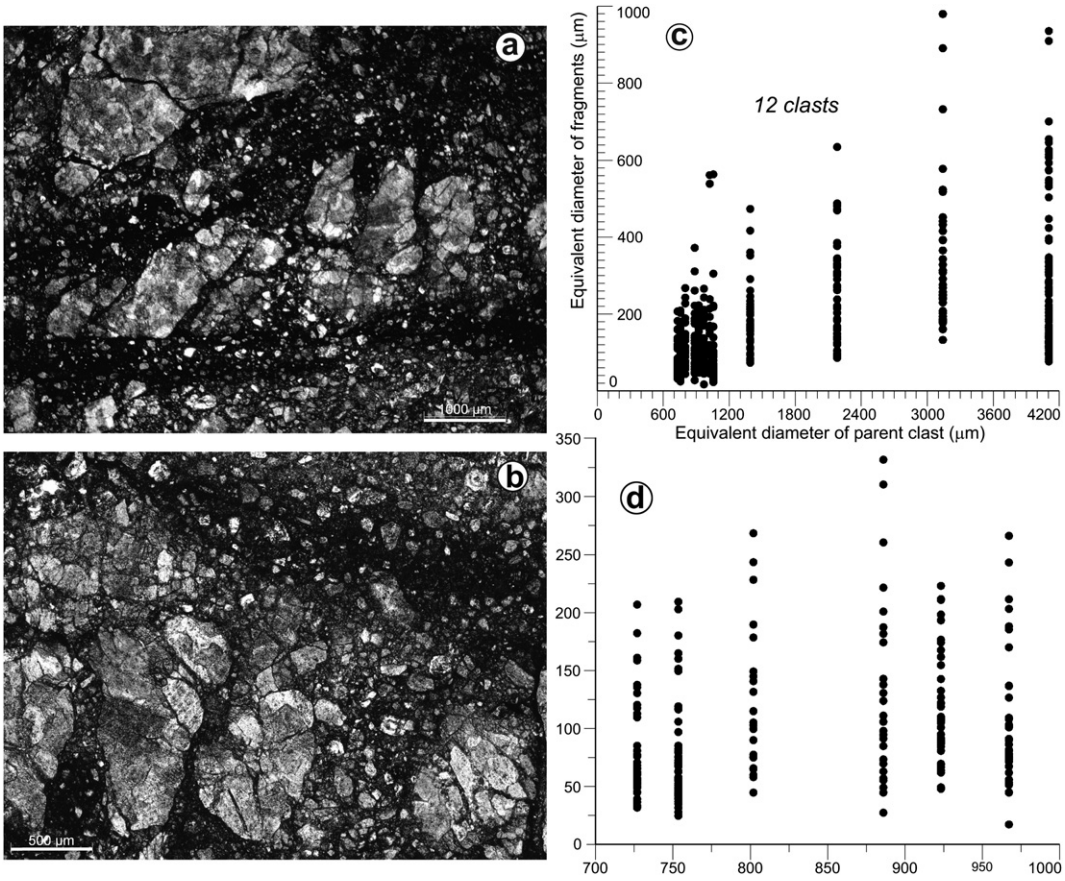

Fig. 3. (a, b) Microphotographs showing microfractured compound clasts surrounded by fine-grained shear bands, which constitute the typical cataclastic fabric in the studied fault breccia. Location of the images is provided in Fig. 2a. (c) Equivalent diameters of parent clasts versus equivalent diameters of the corresponding fracture-bounded fragments. Note the high number of fragments contained in each clast. (d) Detail of the graph in (c) showing the size range of parent clasts that is more pertinent to the laser diffraction size range. A great number of fragments have equivalent diameters close or smaller than about 100 µm.

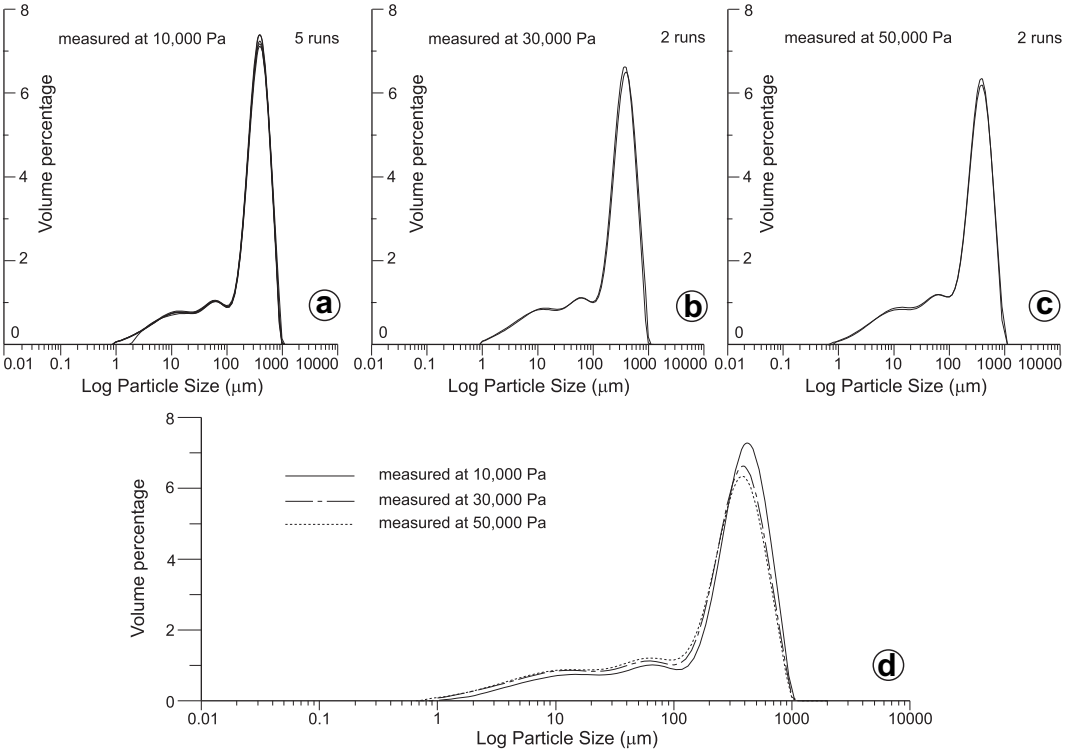

Fig. 4. (a) Granulometric curves obtained by analysing 5 aliquots from sub-sample CABRE1a at 10,000 Pa of compressed air stream. (b) Granulometric curves obtained by analysing 2 aliquots from sub-sample CABRE1b at 30,000 Pa of compressed air stream. (c) Granulometric curves obtained by analysing 2 aliquots from sub-sample CABRE1c at 50,000 Pa of compressed air stream. (d) Comparison among averaged granulometric curves in (a), (b), and (c), respectively.

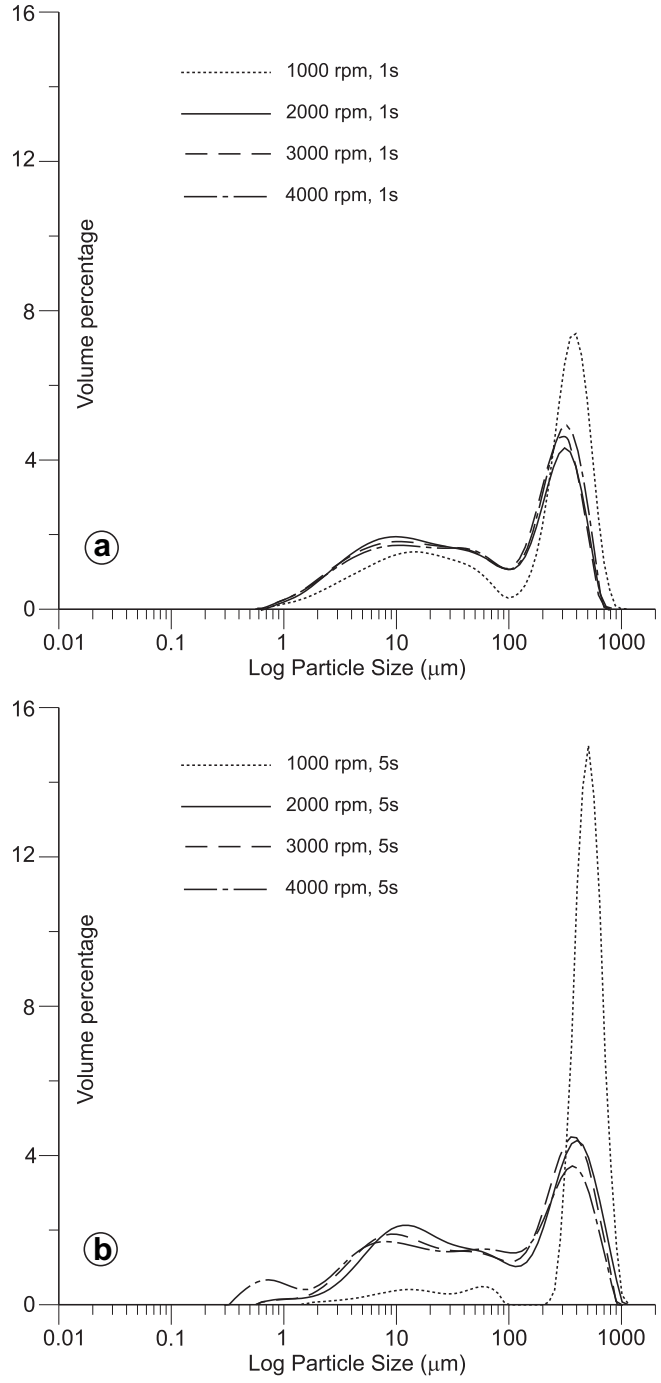

Fig. 5. (a) Comparison among granulometric curves obtained from sub-sample aliquot CABRE1d by averaging 10 runs for each pump speed step, acquired at 1 s of measure run time. (b) Comparison among granulometric curves obtained from sub-sample aliquot CABRE1e by averaging 10 runs for each pump speed step, acquired at 5 s of measure run time.

3.2. Factors influencing data acquisition

Particle size distributions in dry suspensions circulating through the measure cell can be influenced by mechanical factors induced by the dispersion mechanism in the dispersion unit and by the sample recirculation system. In wet suspensions, chemical interactions between sample material, dispersion medium and, when present, dispersing agents, add to mechanical factors. Mechanical sample alteration in the Mastersizer 2000 granulometer equipped with the dry dispersion unit can be associated with pressure intensity in the compressed air stream. When a wet dispersion unit is used, two major factors can produce mechanical bias during measurement runs: (i) centrifugal pump and stirrer speed and, hence, measurement run time and (ii) ultrasonication (e.g. Sperazza et al., 2004). Fast stirring in the sample dispersion unit causes frequent particle–particle and particle–beaker collisions and this can enhance particle fragmentation, particularly in cataclastic rocks, where inherited microfractures are very abundant. The same effect is produced by fast centrifugal pumping during sample recirculation. Ultrasonication provides additional energy to wet dispersions and this can enhance collision-aided particle abrasion and breakage, thus potentially reducing particle size, particularly in fault core rocks.

3.3. Factors influencing light scattering data processing

Since particle size is an indirect result of light scattering data measurements, it can be recomputed by varying optical properties of both analysed material and dispersant liquid. The need for iterative data reprocessing comes from the high variability of the optical properties of rocks and sediments. In particular, the Mie theory utilizes the refractive index (RI) and absorption (ABS) of the dispersed granular material, and the RI of the dispersant liquid. Rocks analysed in this work are essentially monomineralic and this prevents the need of specific studies for RI and ABS determination (e.g. Sperazza et al., 2004). Accordingly, we used RI = 1.60 and ABS = 0.01 for the carbonate cataclastic material. Wet analyses were performed using decalcified tap water and denaturated ethylic alcohol (concentration 90%) as dispersant liquids. Based on the optical properties database available in the Mastersizer 2000 software, an RI = 1.33 was used for the former, while data in alcohol were initially acquired with RI = 1.36 and then reprocessed for comparative purposes with RI = 1.43 and 1.47, respectively.

3.4. Testing strategy

In order to reduce particle breakup, we experimented with different parameters. Different air pressures were tested in the dry dispersion unit. In the wet dispersion unit, the following tests were performed: (i) measurement runs at different pump speed and constant run time; (ii) measurements at given pump speed and run time on the same sub-sample aliquot; (iii) measurements at given pump speed and run time, and with ultrasonication. Moreover, we performed measurements on different sub-sample aliquots at the same boundary conditions (sampling precision tests, Blott et al., 2004). The first three tests were performed on sample CABRE1. Sampling precision was tested on sample CABRE2. Sub-samples from both were sieved at 500 μm. We also performed three long run tests on the coarser fraction of sample CABRE1. They include both particle size and shape analyses and are described in Section 4.

3.5. Dry analyses

A total of nine runs were performed at 10,000 Pa, 30,000 Pa, and 50,000 Pa of compressed air stream on sub-sample aliquots CABRE1a to 1c, respectively (Fig. 4). The corresponding averaged curves illustrate the slight influence of pressure in the compressed air stream. Regardless of the measurement run boundary conditions, particle size distributions are characterized by a dominant modal peak at about 400 μm and by a "tail" of finer particles having volume percentage values lower than about 1% (Fig. 4d).

3.6. Wet analyses – variable pump speed

We tested the influence of the pump speed by performing 10 measurement runs at 1000, 2000, 3000, and 4000 revolutions per minute (rpm), and 1 s (aliquot CABRE1d) and 5 s (CABRE1e) of measurement run time, respectively (Fig. 5). Results showed that data acquired at 1000 rpm were very different from the other ones and showed a much more dominant modal peak, particularly at 5 s of measurement run time. Granulometric curves at higher rpm are much more similar. As a general feature, modal peaks of curves belonging to data acquired at 5 s of measurement run time show a slight coarseward shift, which would not be expected if particle breakage was the main biasing factor during sample recirculation. This supports the inference that 1 s of measurement run time does not ensure the appropriate statistical robustness to the acquired data, and that this uncertainty overcomes the greater particle population alteration produced by longer recirculation times. Among data acquired at 5 s of measurement run time and higher pump speed values, 2000 rpm is the most conservative choice, given the close similarity with the 3000 rpm curve, while data acquired at 4000 rpm show a significant increase of finer particles (Fig. 5b).

3.7. Wet analyses – constant pump speed and run time

To test the effects of mechanical sample alteration during recirculation, we performed 100 measurement runs on sub-sample aliquot CABRE1f, at 2000 rpm of pump speed and 5 s of measurement run time. A selection of granulometric curves every 25 runs is provided in Fig. 6a. It shows that a significant difference occurs between the curve associated with the first measurement run, and the remaining ones, which are very similar. At a greater detail, granulometric curves show that data from the 3rd to the 15th run are very consistent, with a modal peak that is shifted by about 60 μm towards the finer sizes with respect to data collected in the first 3 runs. Comparison with data averaged over 25 runs shows very similar results (Fig. 6b). When 25-run curves are compared for the entire test, their close similarity is well evident, as well as their shift towards finer sizes with respect to the first three-run curve (Fig. 6c).

3.8. Wet analyses – sample ultrasonication

Sub-sample aliquots CABRE1g to 1l were tested at 2000 rpm of pump speed, 5 s of measurement run time, and increasing ultrasonication intensities, from 2.5 to 20 μm of probe tip displacement,

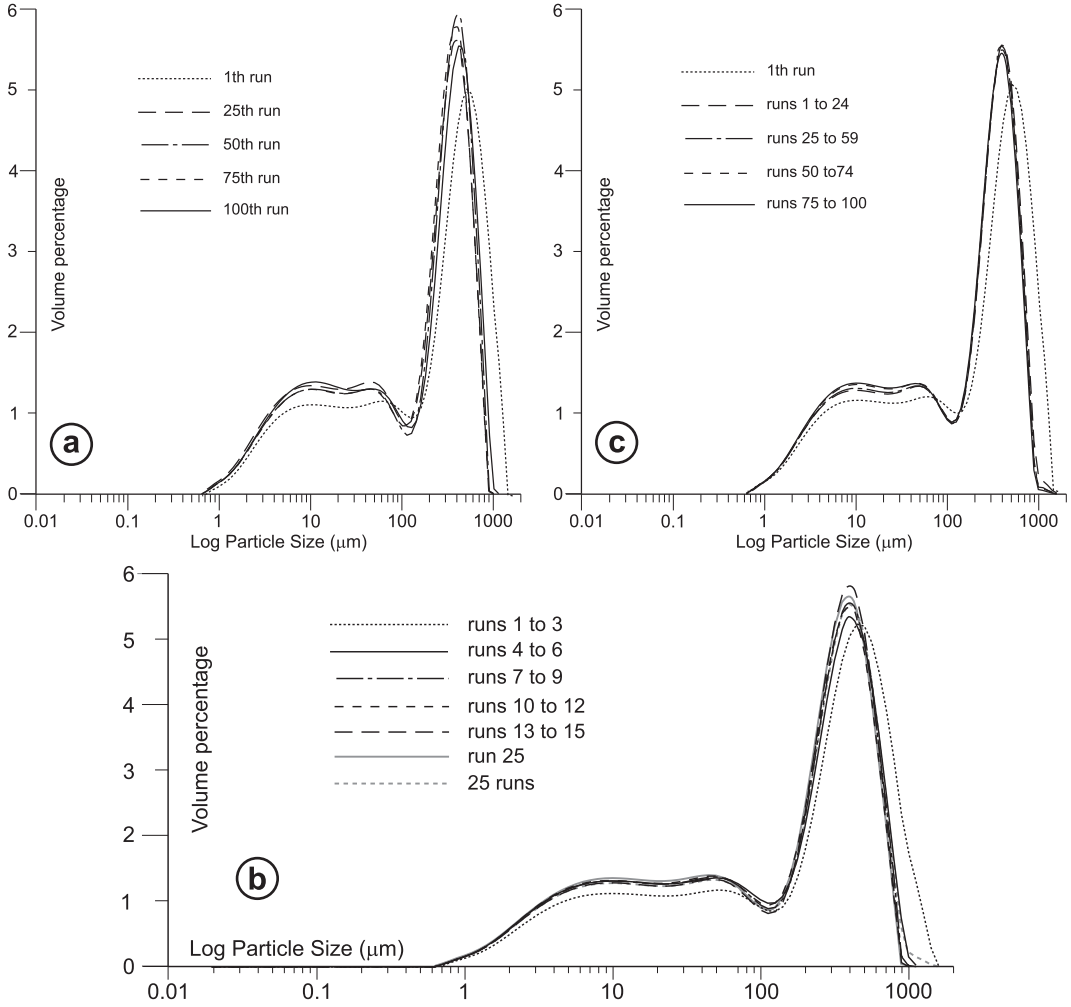

Fig. 6. Results from 100 runs on sub-sample aliquot CABRE1f. (a) Selection of granulometric curves every 25 runs. (b) Results of the first 15 measure runs: granulometric curves are averaged every three runs and compared with the average curve from the first 25 runs, and from the curve from run 25. (c) Granulometric curves produced by data averaging every 25 runs.

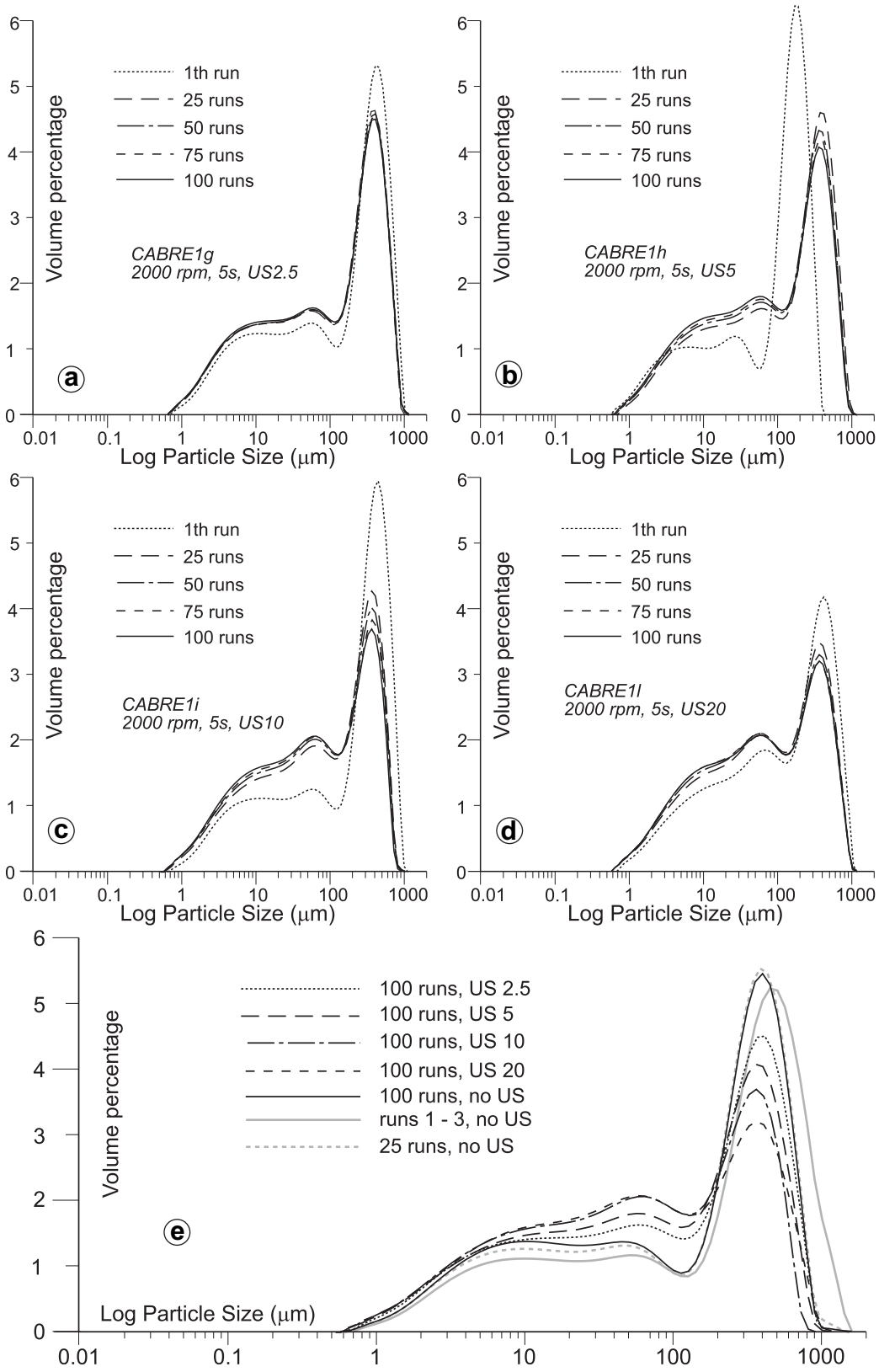

Fig. 7. Results of analyses performed at 2000 rpm of pump speed, 5 s of measurement run time, and different ultrasonication intensities. (a) Sub-sample CABRE1g; 2.5 μm of ultrasonication probe tip displacement. (b) Sub-sample CABRE1h; 5 μm of probe tip displacement. (c) Sub-sample CABRE1i; 10 μm of probe tip displacement. (d) Sub-sample CABRE1l; 20 μm of probe tip displacement. (e) Comparison of 100 run data curves from previous analyses, with the average curve from 100 runs and no ultrasonication (CABRE1f), and with the first 3 run and 25-run curves of the same analysis.

respectively (Fig. 7). In three of the four tests, the first run curve shows a coarseward particle size distribution and a higher modal peak with respect to the following runs. Only in the case of ultrasonication at 5 μm of probe tip displacement, this behaviour is violated and an "anomalous curve" is produced, likely related to a not yet fully established effective sample recirculation. The influence of ultrasonication intensity is negligible on the modal size of the analysed sub-sample aliquots, which is about 390 μm in all cases. On the other hand, this influence is significant on the particle volume percentage associated with the major peak, which decreases from 4.6–4.4% when ultrasonication intensity is 2.5 μm of probe tip displacement, up to 3.5–3.2% when ultrasonication intensity is 20 μm. Modal peak elevation remains almost unvaried during sample recirculation at minimum ultrasonication intensity, regardless of the averaged run numbers. An increase of ultrasonication intensity is accompanied by comparable decreases of modal peak elevations with increasing measurement run numbers, i.e. particle recirculation time, for ultrasonication probe tip displacement of 5 and 10 μm. When the maximum ultrasonication energy is applied to the probe, modal peak decreasing occurs only up to about half of the total measurement runs. This suggests that, at that time, almost all intraparticle flaws exploitable by the total energy applied to recirculating particles were re-activated. Comparison among granulometric curves averaged on total run numbers indicates that the use of ultrasonication decreases the volume percentage of the modal peak values by about 1% at the lowest ultrasonication intensity with respect to data acquired without ultrasonication (Fig. 7e). Doubling ultrasonication intensity causes a corresponding modal peak decrease of about 0.5% and this results in a total decrease of about 40% of the modal peak volume percentage. Finer particles produced by fragmentation of the coarser ones mainly fall in the 5–130 μm size range, being more abundant between 40 μm and 100 μm.

3.9. Wet analyses – denaturated ethylic alcohol

Recomputing data acquired from sub-sample aliquot CABRE1m, at 2000 rpm and 5 s of measurement run time, illustrates the great effect of using denaturated ethylic alcohol instead than water in the dispersion unit (Fig. 8). Curves averaged over 100 runs and computed with RI = 1.36, 1.43, and 1.47 respectively, show similar shapes in the 1–1000 μm size range, while significant differences occur in the finer size classes, particularly when RI = 1.47 is used (Fig. 8a). Fragmentation of particles in the modal peak size range produces finer particles in the 1–100 μm size range, with a great abundance of particles having equivalent diameter of 5–10 μm. Plotting granulometric curves corresponding to runs 1–5, computed for RI = 1.36, and comparing them with the corresponding average curve from 100 measurement runs, and with reference curves acquired in decalcified tap water, show how fast failure is of almost all the "weak fraction" of coarse particles (Fig. 8b).

3.10. Comparative summary

A summary of data obtained from sample CABRE1 is provided in Fig. 9. Regardless of the adopted operating procedures, granulometric curves show a strongly asymmetric shape in a log–normal space, characterized by a major modal peak in the 350–450 μm size range, followed by a long tail towards the finer fractions. Comparison of granulometric curves averaged over the first three measurement runs is designed for minimizing recirculation-related material mechanical alteration. Three major trends can be identified (Fig. 9a). The first one (trend I) corresponds to dry measurements, which are characterized by the smaller and almost

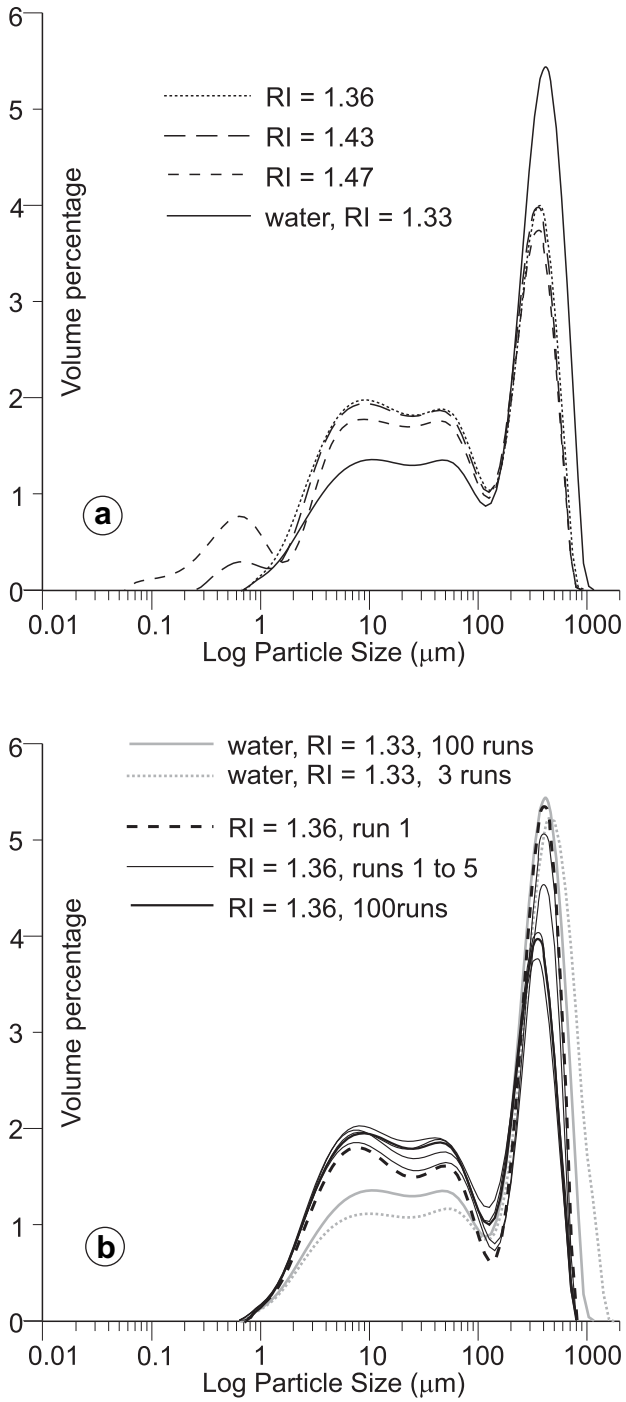

Fig. 8. Data from sub-sample aliquot CABRE1m, acquired at 2000 rpm, 5 s of measurement run time, and denaturated ethylic alcohol as dispersant liquid. (a) Granulometric curves averaged over 100 runs, computed with RI = 1.36, 1.43, and 1.47 respectively. (b) Granulometric curves corresponding to runs 1–5, computed for RI = 1.36 and compared with the corresponding average curve from 100 measurement runs, and with reference curves acquired in decalcified tap water.

continuously decreasing volume percentages in the 2–100 μm size range, and by the largest amounts of coarser particles in the modal peak size (close to 8%). The second trend includes wet measurements performed at 2000 rpm using decalcified tap water as dispersant liquid (trend II). These curves have 4.5–5.3% of modal peak particle volume percentage, flat-lying segments in the 7–100 μm size range, and then decrease to 0 in the 0.2–0.9 μm size

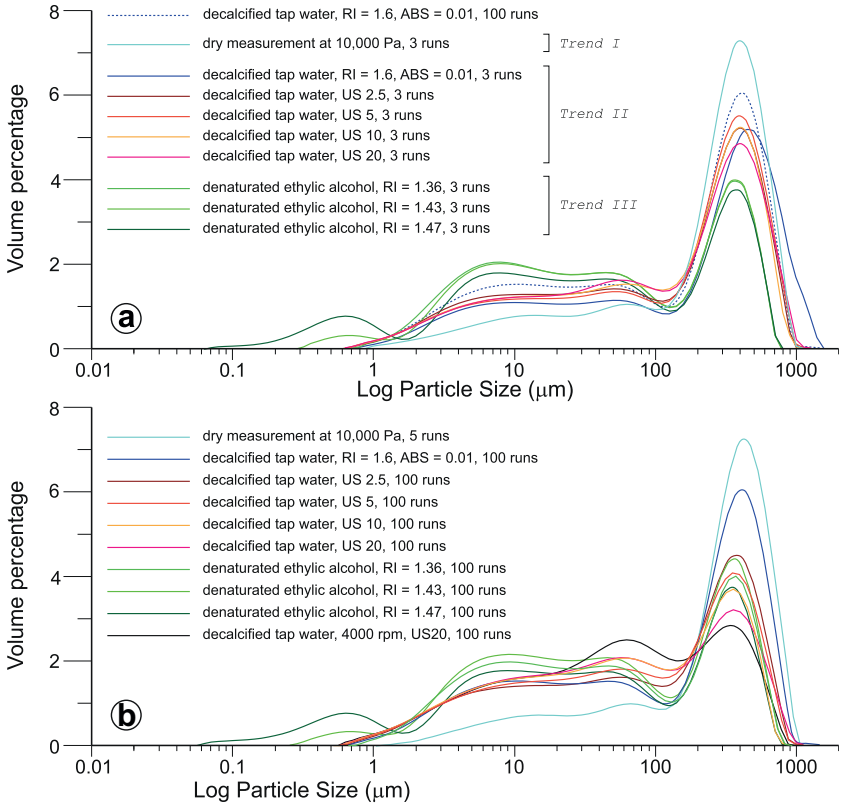

Fig. 9. Comparison among representative granulometric curves obtained from the different tests on sample CABRE1. (a) Curves averaged for the first 3 measurement runs. The reference curve for 100 runs acquired in decalcified tap water, 2000 rpm and 5 s of measurement run time is provided for comparison. (b) Same curves as above but averaged over 100 runs. Only dry measurements are averaged over 5 runs, i.e. the total number of these analyses. See text for details.

range. The third trend includes measurements performed using denaturated ethylic alcohol as dispersant liquid (trend III), which are characterized by the lowest amounts of material in the modal peak size range (about 3.7%), by a gently coarseward dipping central segment, and by significant amounts of finer particles, particularly when RI = 1.47.

When full analysis average curves are compared, the main effects produced by accounting for much longer material recirculation times are the overall decrease of modal peak volume percentage values, and the corresponding increase of material amounts in the central curve segments (Fig. 9b). In this graph, we included the end member curve corresponding to an analysis performed at 4000 rpm and 20 μm of ultrasonication probe tip displacement. This curve is characterized by two almost volumetrically equivalent modal peaks at 65 μm and 350 μm, respectively, followed by a constant decrease of the volume percentages of smaller particles up to zero, which is reached at 0.6 μm. This distribution is fundamentally different from all other ones.

3.11. Sampling precision test

Ten sub-sample aliquots of CABRE2 were analysed at 2000 rpm and 5 s of measurement run time. Twenty-five runs were performed for each aliquot. Comparison of the corresponding granulometric curves averaged over the first 3 runs shows quite similar trends characterized by a broad maximum in the 20–500 μm size range, having two different modal peaks at about 60 μm and 400 μm, respectively (Fig. 10a). When curves averaged over 25 runs are compared, similarity further increases and the reproducibility of results is very good apart from one curve (Fig. 10b).

4. Long run test

Three long run tests were performed on sub-sample aliquots CABRE1n to 1p by performing 500 measurement runs at 2500 rpm of pump speed and 10 s of measurement run time. The corresponding sub-sample was produced by sieving the coarser fraction of sample CABRE1 in the 1000–1700 μm size range. In the first test we used decalcified tap water as dispersant liquid. In the second test we used denaturated ethylic alcohol. The third test was performed using decalcified tap water and ultrasonication at 20 μm of probe tip displacement. At the end of each test, material was dried at 60 °C in a fan assisted oven for 24 h and then analysed again by three runs at 2000 rpm and 5 s of measurement time.

4.1. Particle size evolution

The evolution of particle size distributions during recirculation of CABRE1n is shown in Fig. 11a by a selection of average granulometric curves. The shape of the red curve indicates the fast failure of particles after only 3 measurement runs: the modal peak is at about 900 μm, i.e. 100 μm below the lower sieve mesh aperture during sample preparation. The newly formed finer material is characterized by a subsidiary peak between about 100 μm and 200 μm, followed by a descending tail up to about 3 μm. With increasing the run number, i.e. the recirculation time, the shape of the corresponding curves progressively changes by decreasing the height of the modal peak, by slightly increasing the subsidiary peak, and by forming a third peak in the 1–30 μm size range. Eventually, in the last 114 curves a fourth peak forms by significantly decreasing the finest particle sizes, from about 0.8 μm up to 0.03 μm.

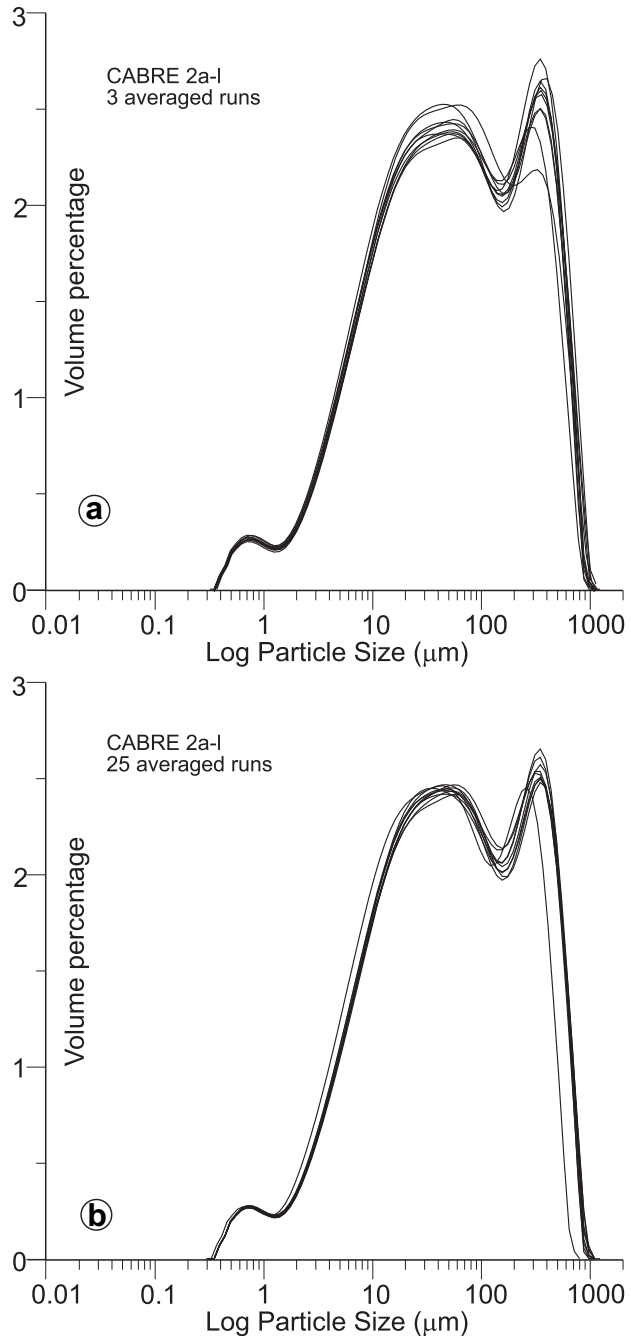

Fig. 10. Results of the sample precision test on sample CABRE2. (a) Granulometric curves averaged over the first 3 runs. (b) Granulometric curves averaged over 25 runs.

Interpretation of these data is not straightforward due to the progressively increasing number of particles in the recirculating suspension, as monitored by the laser obscuration values. The inset graph in Fig. 11a illustrates the progression of this parameter through time, against average particle diameter measured as a volume weighted mean. Mean diameters continuously decrease from about 720 μm to about 250 μm, while laser obscuration increases from about 12% up to about 90%. Laser obscuration is crucial for ensuring the suspension dilution threshold supporting the assumption of the absence of multiple scattering that is required by the Mie diffraction theory (de Boer et al., 1987). By accepting 40% as the maximum admissible laser obscuration value preventing significant multiple scattering, we can identify the first 100 curves as the only reliable ones out of 500. This means that both the second and third subsidiary peaks in the granulometric curves corresponding to data acquired after about 2300 s of recirculation time have to be regarded as artefacts produced by failure of the single scattering assumption in the Mie diffraction theory.

Analysis of data collected in the first 1000 s (40 measurement runs) from sub-sample aliquot CABRE1o provides the most effective possibility to monitor the progression of sample biasing during recirculation (Fig. 11b). The mode of the granulometric curves decreases by about 116 μm, due to the very coarse and very poorly sorted starting size interval of the analysed carbonate particles. The volume percentage values of modal peaks, however, show a significant decrease from about 12% down to about 7%. The abrupt decrease of D_{10} values after less than 250 s of recirculation time is diagnostic of significant particle breakage. Such a decrease then continues at a near constant lower rate up to the end of the data subset.

Progressive subtractions of granulometric curves averaged over constant time intervals provide an additional tool for investigating the evolution of the particle size population through time. The resulting five curves associated with the first 625 s of recirculation time of sub-sample aliquot CABRE1o show a major minimum for sizes slightly greater than 1000 μm, associated with significant fragmentation of the starting material (Fig. 11c). It is accompanied by increasing particle numbers in the 200 μm to 600 μm size range, which in the last two curves broadens up to about 40 μm. A broader maximum then characterizes the finer size segments of all curves, from about 1 μm up to about 30 μm.

Comparison between the first three-run average curve at the beginning of the long run test of CABRE1n, with the corresponding one measured from resulting material after the test, shows a shift of the modal peak towards the finer sizes of about 200 μm, i.e. from 950 to 750 μm (Fig. 12). A very similar behaviour is shown by materials produced after the long run CABRE1p, where ultrasonication was used. It is important to note that at run 286 of this test it was necessary to replace water into the beaker with clean one, in order to set the laser obscuration value at about 15% and allow the experiment to continue. This means that comparison of curves in Fig. 12 is only valid for modal peak size values, while finer particle size data and volume percentages are biased.

4.2. Particle shape characterization

Particle shape analysis was performed by using the Morphologi G3 automated particle characterization system manufactured by Malvern Ltd. This instrument provides high quality gray tone images of loose materials acquired by an optical system equipped with different magnifications from 1× to 50×. The system has a dry powder dispersion system which controls the dispersion pressure, injection time and settling time. A very large number of images can be acquired during each analysis in the 0.5–3000 μm size range, thus allowing a huge number of particle shape data to be computed by image analysis techniques.

In our analyses we used a constant magnification of 5×. Among parameters automatically provided by the Malvern particle characterization system, we identified HS Circularity, Aspect Ratio, and Convexity, normalized in the 0–1 range, as the most effective parameters among available morphological ones to describe the studied carbonate particles. HS (High Sensitivity) Circularity is the ratio of the object's projected area to the square of the perimeter of the object and measures how close the particle's shape is to a perfect circle. Perfectly smoothed circles have an HS Circularity of 1, while strongly elliptical and irregular objects have HS Circularity

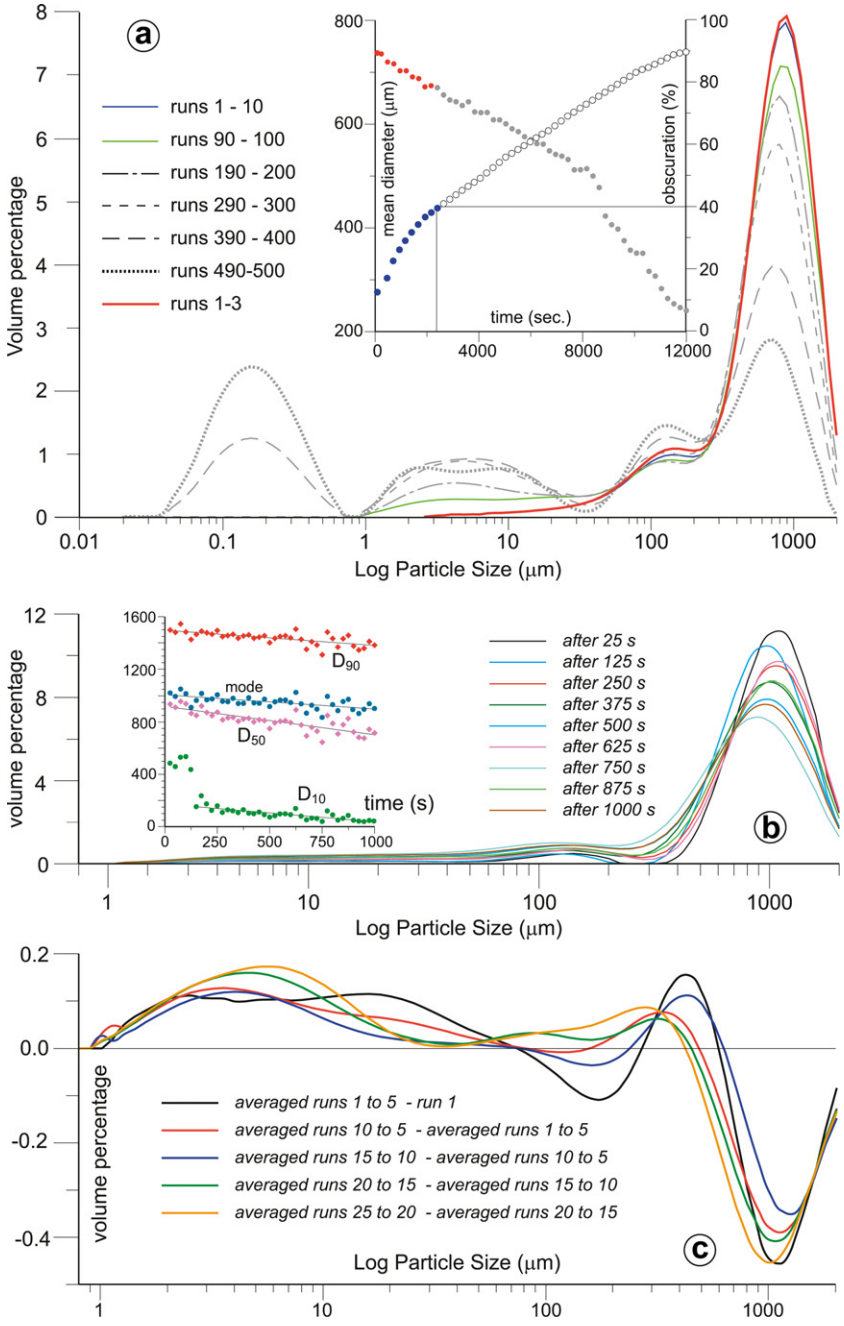

Fig. 11. Results from the long run test. (a) Selected average granulometric curves of sub-sample aliquot CABRE1n, averaged over 10 runs. The inset graph shows the progression of laser obscuration values thought time, against average particle diameter measured as volume weighted mean value. Each point in the graph results from the average of 10 measurement runs. Data in colours pertain to runs acquired with laser obscuration values lower than 40%. (b) Granulometric curves monitoring every 125 s the evolution of particle size during the first 1000 s (40 measurement runs) of the CABRE1o sub-sample aliquot analysis. The inset graph shows the behaviour of D_{10} D_{50}, D_{90}, and modal values. (c) Progressive subtractions of granulometric curves associated with the first 625 s of recirculation time of sub-sample aliquot CABRE1o and averaged over 5 measurement runs. See text for details.

close to 0. Convexity measures the surface roughness of a particle, calculated by dividing the convex hull perimeter by the actual particle perimeter. Very smooth shapes have Convexity close to 1, while very spiky and irregular objects have Convexity closer to 0. Aspect Ratio provides the ratio between the shortest and longest particle axes. A perfect circle has an Aspect Ratio value of 1, while non-equant and elongated particles have Aspect Ratio close to 0.

Comparison between the selected shape parameters of particles before and after the long run test using decalcified tap water as dispersant liquid, shows that the former have lower HS Circularity, lower Convexity, and higher Aspect Ratio values than the latter (Fig. 13). When also particles that underwent ultrasonication during long lasting recirculation are considered, morphological analyses indicate that differences with respect to results without ultrasonication are negligible in terms of HS Circularity and Aspect Ratio. On the other hand, the three populations are clearly distinguishable when Convexity is considered (Fig. 13b).

5. Impact on fractal dimensions

Differences among granulometric curves obtained from the same sample by using different operating procedures result in

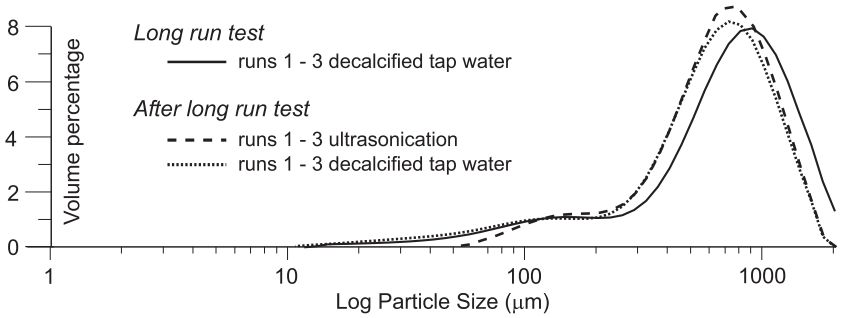

Fig. 12. Comparison between particle shape distribution of sub-sample aliquot CABRE1n at the beginning of the long run test (runs 1–3) and that of materials that resulted after the test, were dried and then measured again. See text for details.

different fractal dimensions (D) when these data are analysed in bilogarithmic graphs. Results from data associated with granulometric curves in Fig. 9a show very good linear fits in bilogarithmic graphs and, consequently, statistically robust D values (Fig. 14). The lowest fractal dimension ($D = 2.54$) is provided by dry measurements at 10,000 Pa of air pressure. The highest one ($D = 2.81$) pertains to data acquired using denaturated ethylic alcohol as dispersant liquid and RI = 1.36. The remaining seven D values are very similar, regardless of different operating procedures and dispersant RI values. Comparison with data obtained from the same analyses averaged over 100 runs (data in Fig. 9b) indicates a generalized increase of D values with increasing recirculation time (Fig. 15a). The influence of this parameter is higher when decalcified tap water is the dispersant liquid with and without ultrasonication. In the former case, when probe tip displacement is 20 μm, the corresponding fractal dimension is $D = 2.88$.

The evolution of D values during the long run test of sub-sample aliquot CABRE1n shows a rapid increase up to about 2200 s of recirculation time, from the averaged first three runs, up to data averaged from run 90 to 100 (Fig. 15b). With increasing particle recirculation time, D values continue to increase at a lower rate. These fractal dimensions, however, pertain to data biased by laser obscuration values higher than 40%.

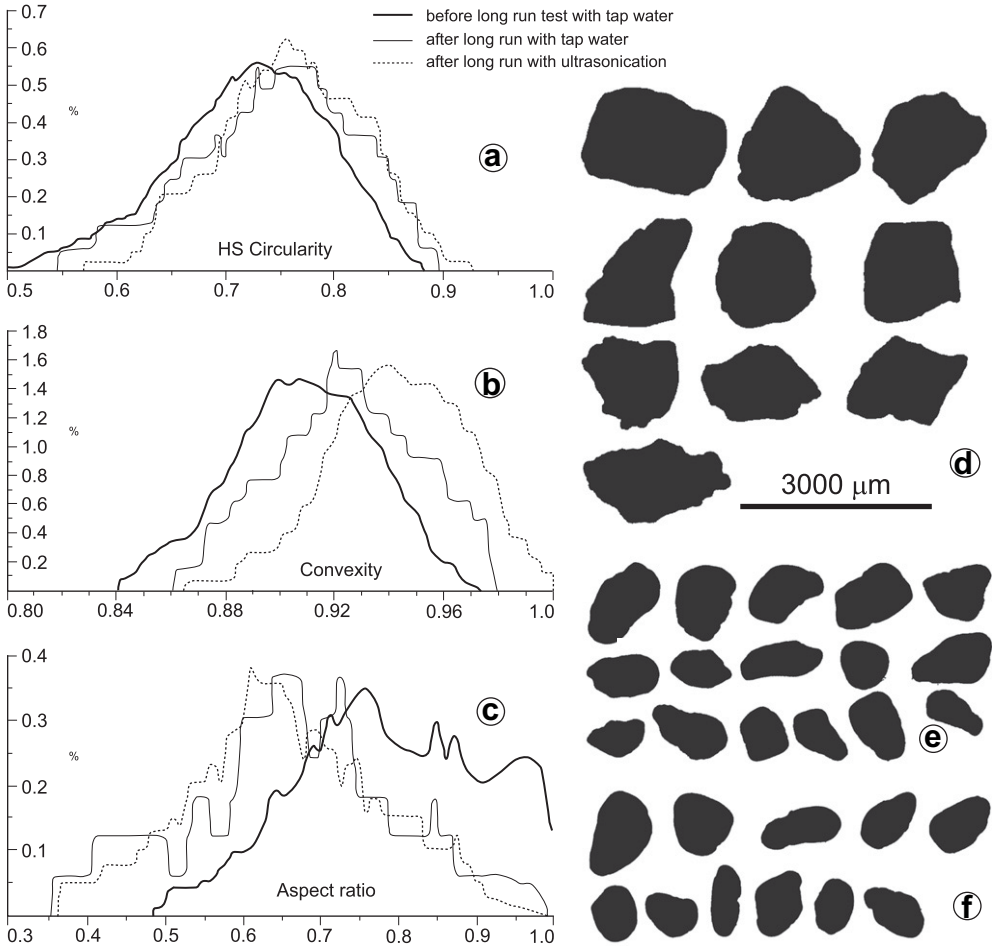

Fig. 13. Comparison among morphometric data of particles before and after the long run test using decalcified tap water as dispersant liquid (CABRE1n) and ultrasonication during recirculation (CABRE1p). (a) HS Circularity data. (b) Convexity data. (c) Aspect Ratio data. (d) 2D shapes of coarsest particles in sub-sample aliquot CABRE1n before the long run test. (e) 2D shapes of coarsest particles in sub-sample aliquot CABRE1n after the long run test. (f) 2D shapes of coarsest particles in sub-sample aliquot CABRE1p after the long run test.

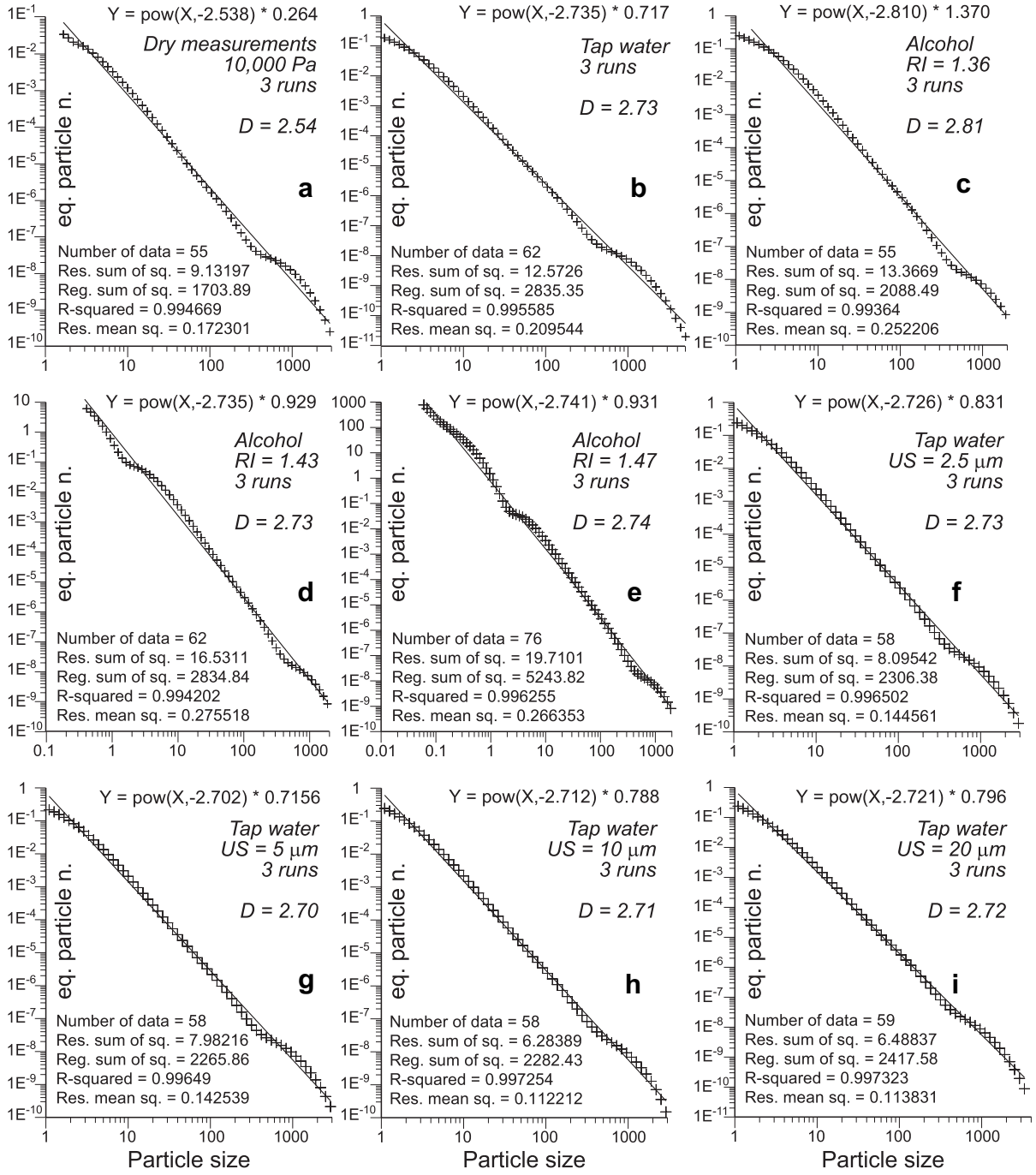

Fig. 14. Comparison among data averaged over the first 3 measurement runs of the different tests on sample CABRE1 (data in Fig. 9a). Equivalent particle numbers were computed following Storti et al. (2003) and plotted against size in bilogarithmic graphs. Best fit lines of the power law distributions and their statistical parameters are provided for each graph. (a) Dry measurements at 10,000 Pa. (b) Decalcified tap water, 2000 rpm, 5 s of measurement run time. (c) Denaturated ethylic alcohol, 2000 rpm, 5 s of measurement run time, RI = 1.36. (d) Denaturated ethylic alcohol, 2000 rpm, 5 s of measurement run time, RI = 1.43. (e) Denaturated ethylic alcohol, 2000 rpm, 5 s of measurement run time, RI = 1.47. (f) Decalcified tap water, 2000 rpm, 5 s of measurement run time, 2.5 μm of ultrasonication probe tip displacement. (g) Decalcified tap water, 2000 rpm, 5 s of measurement run time, 5 μm of ultrasonication probe tip displacement. (h) Decalcified tap water, 2000 rpm, 5 s of measurement run time, 10 μm of ultrasonication probe tip displacement. (i) Decalcified tap water, 2000 rpm, 5 s of measurement run time, 20 μm of ultrasonication probe tip displacement.

6. Discussion

Comparison between particle size distributions obtained from sample CABRE1 by dry and wet operating procedures provides meaningful insights for the mechanical response of carbonate cataclastic rocks during laser diffraction granulometry. Dry analyses provided very similar results and the coarser particle size distributions, which likely represent very close approximations of the actual size distribution. On the other hand, wet analyses provided finer particle size distributions. The only exceptions are data acquired at very low pump speed, which are characterized by abnormally high volume percentages of coarse particles, likely caused by ineffective recirculation in the dispersion unit. A progressive decrease of representative percentile, mean diameter, and mode values, systematically occurred during wet measurement runs. In particular, a major size decrease occurred in

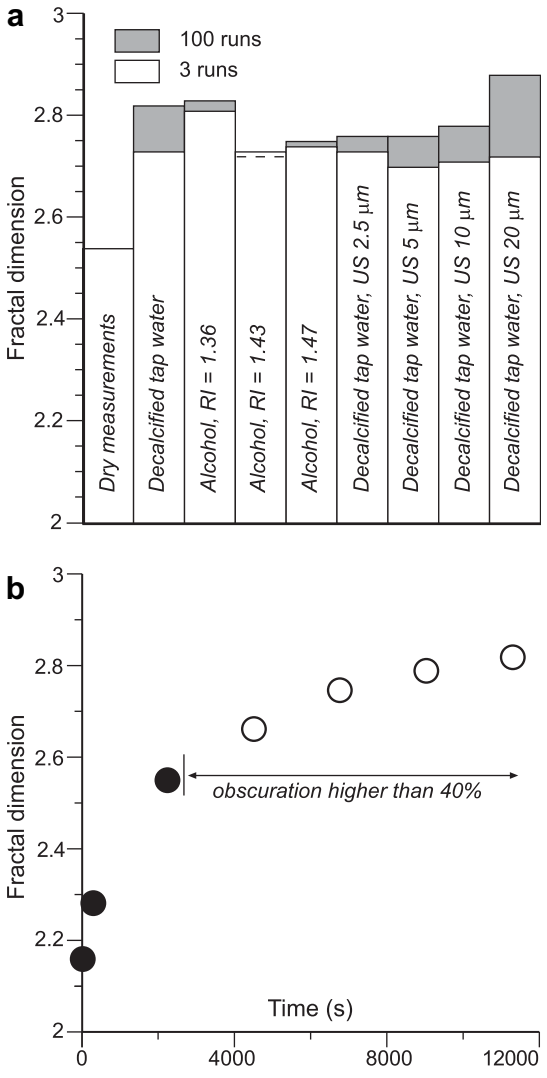

Fig. 15. (a) Comparison among fractal dimensions obtained from different tests on sample CABRE1, being data averaged over 3 and 100 runs, respectively. (b) Evolution of D values during the long run test of sub-sample aliquot CABRE1n. See text for details.

the first few runs (Fig. 6). This evidence can result from either initially ineffective recirculation in the dispersion unit, or by rapid breakage of coarse particles. The first hypothesis can be ruled out as a general case by noting that the same phenomenon occurred in almost all tests, regardless of pump speed and ultrasonication. Instead, coarse particle disintegration is supported by the interpretation of the D values from the thin section analysis of the same rock. The actual particle size distribution, including compound clasts, gave $D = 2.52$, i.e. a fractal dimension very similar to that obtained by dry laser diffraction from the loose counterpart rock ($D = 2.54$). The retouched particle size distribution, obtained by manually disintegrating all compound clasts available in the microphotographs, gave $D = 2.87$, which again compares very well with the fractal dimension obtained by wet laser diffraction and 20 μm of ultrasonication probe tip displacement ($D = 2.88$), i.e. a very invasive procedure, suitable to enhance compound clast disintegration. Particle fragmentation is also supported by results from morphological analyses of particles before and after the long run test. They indicate that sample recirculation in the dispersion unit caused elongate particle breakage perpendicularly to the long axis (aspect ratio decreases), and particle abrasion and smoothing by chipping, as suggested by the increase of both convexity and HS circularity.

Occurrence of widespread particle disintegration is explained by the peculiar fabric of cataclastic rocks derived from massive protoliths, like platform carbonates. In fact, in this case the meaning of particle is not straightforward and depends on the relative strength distribution along cleavage and microfracture sets as a function of the applied stress (e.g. Sammis et al., 1987). The result is an ephemeral cataclastic fabric characterized by the transient nature of coarser compound clasts that, due to intense internal fracturing, are prone to disintegrate into numerous finer fragments. Three-dimensional numerical simulations of cataclasis in granular material reproduced comparable parent clast disintegration with increasing shear (Mair and Abe, 2008). Calculations from thin section image analysis provide parent clast versus pertinent fragment equivalent diameter distributions that support the evolution of the granulometric curves obtained with increasing sample mechanical stress, i.e. the failure of large clasts (equivalent diameter lower than 1000 μm) produces a significant increase of particles smaller than 100 μm.

The different capability of wet and dry dispersion systems to exploit intense intraparticle microfracturing characterizing ephemeral cataclastic fabrics can explain the difference of results from the two classes of operating procedures in laser diffraction granulometry of cataclastic rocks. Liquid dispersants can wet microfractures and help cohesion loss, thus favouring compound clast disintegration. Fracture aperture thresholds that can be permeated by capillarity depend on the surface tension of the adopted dispersant liquids. The lower is the surface tension, the higher is the particle disintegration capability of dispersant liquids.

The mechanical behaviour of ephemeral cataclastic fabrics inferred by comparing results from thin section analysis, from particle optical morphometry, and from laser diffraction particle size analysis, can provide insights for that of natural fault breccia and gouge undergoing deformation at different environmental conditions. In particular, three main scenarios can be schematically described (Fig. 16). (a) At shallow depth and low differential stress conditions, many microfractured compound clasts can survive as single coarse particles during shear. This is expected to produce particle size distributions characterized by a dominant modal peak in the corresponding granulometric curves (trend I), comparable to results from dry laser diffraction analyses of sample CABRE1. (b) Increasing differential stress causes failure of many compound clasts and consequent production of abundant smaller particles. Granulometric curves expected for these fault rocks have an increased number of particles in the size fractions smaller than about 100 μm (trend II). This is comparable to results from moderately invasive wet laser diffraction analyses of sample CABRE1. Eventually, almost complete failure of compound clasts can occur during long lasting shearing of fault core rocks (c), resulting in a dramatic drop of the coarse size modal peak and in a large increase of smaller particles (trend III). Such a particle size distribution is expected to be comparable to results from highly invasive laser diffraction analyses of sample CABRE1. The evolution of the cataclastic fabric includes particle morphology changes towards more smoothed and rounded shapes, associated with failure of coarser clasts and rolling-related particle chipping and abrasion (e.g. Storti et al., 2007). This implies that, when cementation is negligible, ephemeral cataclastic fabrics likely favor effective fault weakening behaviors with increasing shear deformation and differential stress.

Very different results are expected to be provided by using either minimally or significantly invasive operating procedures in laser diffraction particle size analysers. This can explain the great discrepancies of particle size distributions obtained from

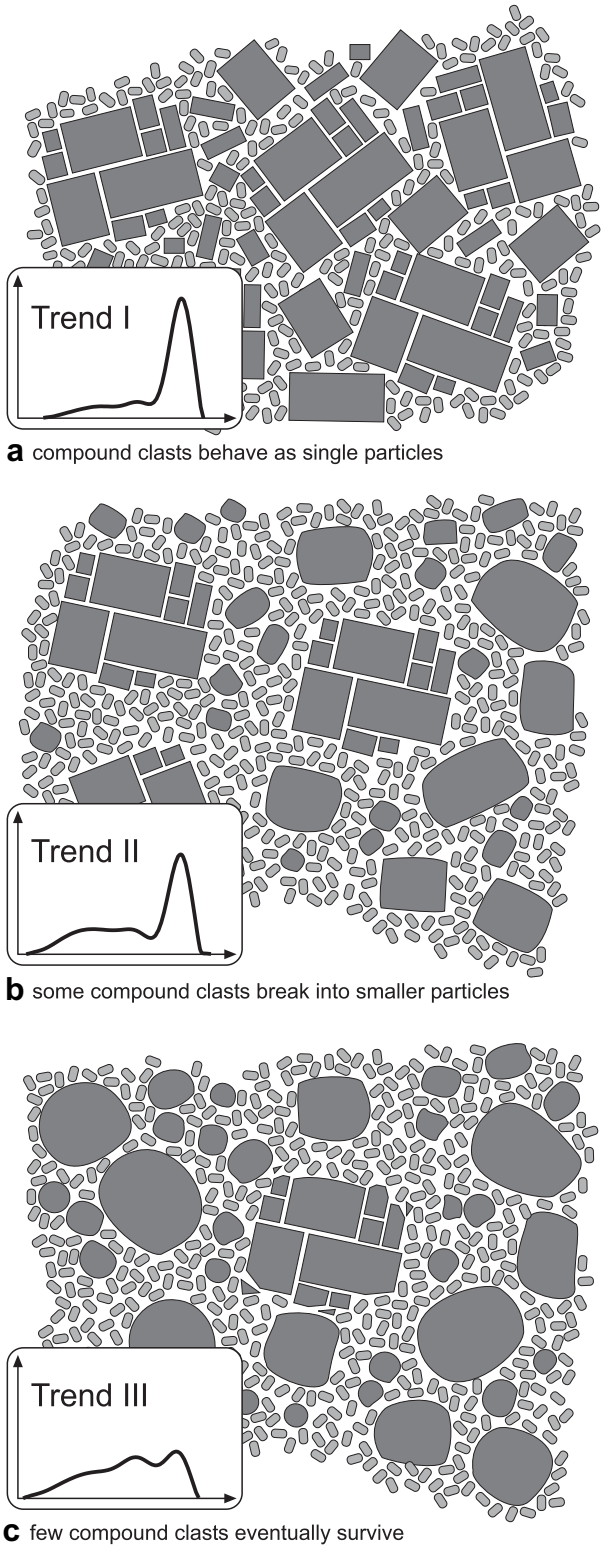

Fig. 16. Conceptual cartoon showing the inferred response of the ephemeral cataclastic fabric of carbonate cataclastic breccias during deformation at different environmental conditions. See text for details.

microscopic and sieve analyses (e.g. Sammis et al., 1986; Blenkinsop, 1991; Storti et al., 2003), and from invasive laser diffraction analyses (e.g. Wilson et al., 2005), respectively. Information from both invasive and minimally invasive analytical strategies can be both meaningful for better understanding the faulting process. However, the mechanical properties of fault rocks are governed by their actual cataclastic fabrics (e.g. Paterson and Wong, 2005). Accordingly, the less invasive operating procedures should be routinely used in laser diffraction granulometry of cataclastic rocks. This because our results show that the variability of *D* values obtained by analysing the same sample with different operating procedures is of the same order of magnitude of that associated with the transition from low- to high-deformation fault breccias and gouges (Sammis and King, 2007) and, consequently, wrong inferences can be easily made. A major drawback of this is that information on preliminary tests performed to select appropriate operating procedures, and on sensitivity tests, should be always associated with granulometric curves of cataclastic breccias.

Results illustrated in this work may question the validity of particle size data produced by sample ultrasonication in wet dispersions preceding sieving (e.g. Storti et al., 2003). The use of identical ultrasonication time and intensity in all analyses supports the effectiveness of relative data comparison among the obtained *D* values. On the other hand, actual particle size distributions might be slightly fineward biased and, consequently, the corresponding *D* values might be slightly overestimated. This may suggest that the very few *D* values exceeding 3.0 that were obtained from cataclastic carbonate fault breccias analysed by ultrasonication preceding sieving (Billi et al., 2003; Storti et al., 2003; Billi and Storti, 2004; Billi, 2005, 2007) may have suffered some ultrasonication-related fineward biasing, being their actual *D* values not higher than 3.0. This would allow them to fit into the theoretically predicted power law distribution of particle sizes produced in high-deformation shear bands (Sammis and King, 2007).

7. Conclusions

Different operating procedures in laser diffraction particle size distribution analysis of loose and poorly cohesive carbonate fault breccia and gouge derived from massive protoliths highlighted the following points.

(1) Dry dispersions provided the coarser particle size distributions, characterized by significantly smaller amounts of finer particles, likely providing the best approximation of the actual size distributions in these cataclastic rocks. Wet dispersions unavoidably caused fineward biasing of particle size distributions, which increased when recirculation pump speed was increased, when ultrasonication was used during material recirculation, and when dispersant liquids having surface tension lower than water were used.

(2) Integration of particle size distributions from thin section analysis on the same rocks impregnated into epoxy, with optical morphometric analyses on the loose counterparts, and their comparison with laser diffraction particle size distributions, supports disintegration of coarse particles as the dominant mechanism to explain the fineward trends in wet laser granulometry, ruling out ineffective particle recirculation in the dispersion unit as an alternative solution.

(3) Coarse particle disintegration is favored by the cataclastic microstructure, which consists of intensely microfractured large particles that can survive as compound clasts or easily fail into several smaller particles, depending on the environmental conditions of deformation. This highly susceptible and transient microstructure constitutes an ephemeral cataclastic fabric that, when cementation is negligible, likely favors fault weakening behaviors.

(4) Invasive operating procedures in laser diffraction particle size analysers can cause disintegration of ephemeral cataclastic fabrics in fault core rocks. It follows that, depending on the

adopted analytical procedure, the fractal dimensions of particle size distributions from these rocks can have a variability of the same magnitude of that theoretically predicted for low- and high-deformation fault breccia and gouge (e.g. Sammis and King, 2007). This highlights the need to carefully determine the most appropriate operating procedure for laser diffraction particle size determinations from granular fault core rocks, possibly accompanied by microscopic analysis of the same materials. Systematic support of laser diffraction granulometric data by preliminary test results performed to select the adopted operating procedure is necessary to prevent misleading data interpretation.

Acknowledgements

This paper strongly benefitted from careful and constructive reviews by S.J. Blott and C. Marone, and from the very effective editorial advice by T. Blenkinsop, which allowed us to significantly improve and better organize the original manuscript. Funding for this work was provided by the “Roma Tre” University Laboratory Upgrade Programme, grants to F. Storti, and by the Italian MIUR (Ministero dell'Istruzione, dell'Università e della Ricerca). We are grateful to Malvern Instruments Ltd. (particularly to P. Kippax and A. Virden) and to Alfatest s.r.l. (particularly to M. Congia and V. Polchi), for their technical support and advice. This paper is dedicated to the memory of Renato Funiciello, who was our mentor since the Geology Department was established at “Roma Tre” University.

References

Anthony, J.L., Marone, C., 2005. Influence of particle characteristics on granular friction. Journal of Geophysical Research 110, B08409. doi:10.1029/2004JB003399.

Antonellini, M., Aydin, A., 1995. Effect of faulting on fluid flow in porous sandstones: geometry and spatial distribution. American Association of Petroleum Geologists Bulletin 79, 642–671.

Ben-Zion, Y., Sammis, C.G., 2003. Characterization of fault zones. Pure and Applied Geophysics 160, 677–715.

Beuselinck, L., Govers, G., Poesen, J., Degraer, G., Froyen, L., 1998. Grain-size analysis by laser diffractometry: comparison with the sieve-pipette method. Catena 32, 193–208.

Billi, A., 2005. Grain size distribution and thickness of breccia and gouge zones from thin (<1 m) strike-slip fault core in limestone. Journal of Structural Geology 27, 1823–1837.

Billi, A., 2007. On the extent of size range and power law scaling for particles of natural carbonate fault cores. Journal of Structural Geology 29, 1512–1521.

Billi, A., Storti, F., 2004. Fractal distributions of particle size in carbonate cataclastic rocks from the core of a regional strike-slip fault. Tectonophysics 384, 115–128.

Billi, A., Di Toro, G., 2008. Fault-related carbonate rocks and earthquake indicators: recent advances and future trends. In: Landowe, S.J., Hammler, G.M. (Eds.), Structural Geology: New Research. Nova Science Publishers, Hauppauge, New York, pp. 1–24.

Billi, A., Storti, F., Salvini, F., 2003. Particle size distributions of fault rocks in fault transpression: are they related? Terra Nova 15, 61–66.

Blenkinsop, T.G., 1991. Cataclasis and processes of particle size reduction. Pure and Applied Geophysics 136, 59–86.

Blott, S.J., Croft, D.J., Pye, K., Saye, S.E., Wilson, H.E., 2004. Particle size analysis by laser diffraction. In: Pye, K., Croft, D.J. (Eds.), Forensic Geoscience: Principles, Techniques and Applications. Geological Society, London, Special Publication, 232, pp. 63–73.

Borg, I., Friedman, M., Handin, J., Higgs, D.V., 1960. Experimental deformation of St. Peter sand: a study of cataclastic flow. Geological Society of America Memoir 79, 133–191.

Caine, J.S., Evans, J.P., Forster, C.B., 1996. Fault zone architecture and permeability structure. Geology 24, 1025–1028.

D'Agostino, N., Chamot-Rooke, N., Funiciello, R., Jolivet, L., Speranza, F., 1998. The role of pre-existing thrust faults and topography on the styles of extension in the Gran Sasso range (central Italy). Tectonophysics 292, 229–254.

de Boer, G.B.J., de Weerd, C., Thoenes, D., Goossens, H.W.J., 1987. Laser diffraction spectrometry: Fraunhofer diffraction versus Mie scattering. Particle Characterization 4, 138–146.

Engelder, J.T., 1974. Cataclasis and the generation of fault gouge. Geological Society of America Bulletin 85, 1515–1522.

Evans, J.P., Forster, C.B., Goddard, J.V., 1997. Permeability of fault-related rocks, and implications for hydraulic structure of fault zones. Journal of Structural Geology 19, 1393–1404.

Fossen, H., Schultz, R.A., Shipton, Z.K., Mair, K., 2007. Deformation bands in sandstone: a review. Journal of the Geological Society (London) 164, 755–769.

Heilbronner, R., Keulen, N., 2006. Grain size an grain shape analysis of fault rocks. Tectonophysics 427, 199–216.

Hadizadeh, J., 1994. Interaction of cataclasis and pressure solution in a low-temperature carbonate shear zone. Pure and Applied Geophysics 143, 255–280.

Mair, K., Abe, S., 2008. 3D numerical simulations of fault gouge evolution during shear: grain size reduction and strain localization. Earth and Planetary Science Letters 274, 72–81.

Mair, K., Frye, K.M., Marone, C., 2002. Influence of grain characteristics on the friction of granular shear zones. Geophysical Research Letters 107 doi:1029/2001JB000516.

Marone, C., Kilgore, B., 1993. Scaling of the critical slip distance for seismic faulting with shear strain in fault zones. Nature 362, 618–622.

Marone, C., Scholz, C.H., 1989. Particle-size distribution and microstructures within simulated fault gouge. Journal of Structural Geology 11, 799–814.

Monzawa, N., Otsuki, K., 2003. Comminution and fluidization of granular fault materials: implications for fault slip behavior. Tectonophysics 367, 127–143.

Morgan, J.K., 1999. Numerical simulations of granular shear zones using the distinct element method. 2. Effects of particle size distribution and interparticle friction on mechanical behavior. Journal of Geophysical Research 104, 2721–2732.

Panozzo, R., 1982. Determination of size distributions of spheres from size distributions of circular sections by Monte Carlo methods. Microscopica Acta 86, 37–48.

Paterson, M.S., Wong, T.-f., 2005. Experimental Rock Deformation – the Brittle Field, second ed. Springer, Berlin.

Rawling, G.C., Goodwin, L.B., 2003. Cataclasis and particulate flow in faulted, poorly lithified sediments. Journal of Structural Geology 25, 317–331.

Reches, Z., Dewers, T.A., 2005. Gouge formation by dynamic pulverization during earthquake rupture. Earth and Planetary Science Letters 235, 361–374.

Sammis, C.G., King, G.C.P., 2007. Mechanical origin of power law scaling in fault zone rock. Geophysical Research Letters 34, L04312. doi:10.1029/2006GL028548.

Sammis, C.G., Ben Zion, Y., 2008. Mechanics of grain-size reduction in fault zones. Journal of Geophysical Research 113, B02306. doi:10.1029/2006JB004892.

Sammis, C.G., Osborne, R.H., Anderson, J.L., Banerdt, M., White, P., 1986. Self-similar cataclasis in the formation of fault gouge. Pure and Applied Geophysics 124, 54–77.

Sammis, C.G., King, G., Biegel, R., 1987. The kinematics of gouge deformation. Pure and Applied Geophysics 125, 777–812.

Sperazza, M., Moore, J.N., Hendrix, M.S., 2004. High-resolution particle size analysis of naturally occurring very fine-grained sediment through laser diffractometry. Journal of Sedimentary Research 74, 736–743.

Storti, F., Billi, A., Salvini, F., 2003. Particle size distributions in natural carbonate fault rocks: insights for non-self-similar cataclasis. Earth and Planetary Science Letters 206, 173–186.

Storti, F., Balsamo, F., Salvini, F., 2007. Particle shape evolution in natural carbonate granular wear material. Terra Nova 19, 344–352.

Torabi, A., Fossen, H., Alaei, B., 2008. Application of spatial correlation functions in permeability estimation of deformation bands in porous rocks. Journal of Geophysical Research 113, B08208. doi:1029/2007JB005455.

Tullis, T.E., Weeks, J.D., 1986. Constitutive behavior and stability of frictional sliding of granite. Pure and Applied Geophysics 124, 383–414.

Turcotte, D.L., 1986. Fractals and fragmentation. Journal of Geophysical Research 91, 1921–1926.

Wilson, B., Dewers, T., Reches, Z., Brune, J., 2005. Particle size and energetics of gouge from earthquake rupture zones. Nature 434, 749–752.

Zhang, S., Tullis, T.E., 1998. The effect of fault slip on permeability anisotropy in quartz gouge. Tectonophysics 295, 41–52.